DCSr-NL: A Novel Method to Semiquantitatively Probe the Growth Rate of Nacre

Li Yi, Bing Zou, Liping Xie, and Rongqing Zhang*

Cite This: *ACS Omega* 2022, 7, 23624−23633

Read Online

ACCESS | Metrics & More | Article Recommendations | Supporting Information

ABSTRACT: Matrix proteins play critical roles in regulating the prismatic and nacreous layer formation in the shell. However, due to the dearth of *in vivo* experiments, their specific roles during shell formation are still unclear. In this study, a new method to detect the content of Sr in the nacreous layer (DCSr-NL), which can semiquantitatively measure the nacreous growth rate, has been proposed. *In vitro* experiments show that during *in vitro* crystallization, the Sr element can replace Ca partially, resulting in isomorphism. *In vivo* experiments show that the best labeling conditions are when the Sr/Ca in seawater is 0.3, at 24 °C, and at 4 days of culture. Although a surface morphological difference in the inner layer of nacre is seldom detected by scanning electron

microscopy (SEM), knockdown of the classical gene nacrein or unknown gene NU9, combined with DCSr-NL, shows that both significantly decrease the nacreous layer formation rate. The knockdown of the classical gene Pif177 or unknown genes NU3 or MRPN affects the surface morphology and decreases the nacreous layer formation rate. In general, thanks to DCSr-NL, we can efficiently analyze the growth rate of the nacre with or without morphological changes by SEM, and it is of considerable significance for exploring the target gene's function in forming the nacre *in vivo*.
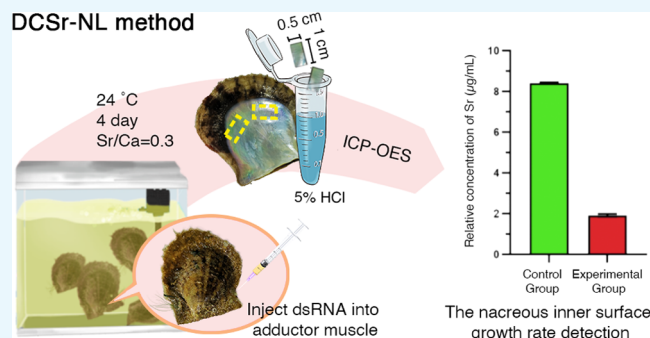
INTRODUCTION

The nacreous layer of mollusk shells has excellent mechanical properties; its mechanical strength is 3000 times that of calcium carbonate crystals,[1,2] inspiring the design of biomimetic materials due to its hierarchical structures at multiple scales.[3−7] It comprises 95% calcium carbonate and about 5% organic matter, including matrix proteins, polysaccharides, and lipids.[5] Studies have shown that matrix proteins play an essential role in regulating the crystal morphology, growth, nucleation, and orientation during shell formation.[8−11] It is expressed and secreted by the mantle tissue, which can be dissected into three parts: mantle edge (ME), mantle pallial (MP), and mantle center (MC).[12,13] The matrix proteins secreted from ME mainly participate in the shell prism formation while those secreted from the other sections are involved in shell nacre growth.[13]

At present, the methods commonly used to study the function of matrix proteins in biomineralization mainly depend on *in vitro* explorations. In the early days, researchers studied whether the proteins from the biological molecules have a regulatory effect on calcite and aragonite formation, crystal phase switching, and orientation in mollusk shells by optical microscopy, transmission electron microscopy, Fourier transform infrared (FTIR) spectroscopy, Raman spectroscopy, X-ray diffraction, and so on, after directly adding the bioorganic macromolecules extracted from shells to the *in vitro*-constructed calcium carbonate crystallization system.[2,14] With

the expansion of research, it was discovered that proteins with aspartate-rich regions are responsible for the controlled crystallization of $Ca[CO_3]$ layers of shells[15,16] and proven that poly-aspartate (pAsp) alone could regulate the formation of calcium carbonate crystals.[15,17] However, as results from *in vitro* experiments have a more auxiliary effect in elucidating the function of matrix proteins, it is necessary to determine their role in shell formation through *in vivo* functional experiments. In 2009, Suzuki et al. applied RNAi to study mollusks for the first time. Also, by combining with scanning electron microscopy (SEM), they successfully proved that the matrix protein Pif177 has a significant regulatory effect on the morphology of the nacre surface *in vivo*.[11] Until now, the combination of RNAi and SEM observations has proved that multiple matrix proteins have a regulatory effect on the morphology of shells.[11,18,19]

However, this classical approach limited the previously published studies to matrix proteins with more pronounced differences in the surface morphology before and after RNA
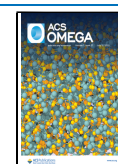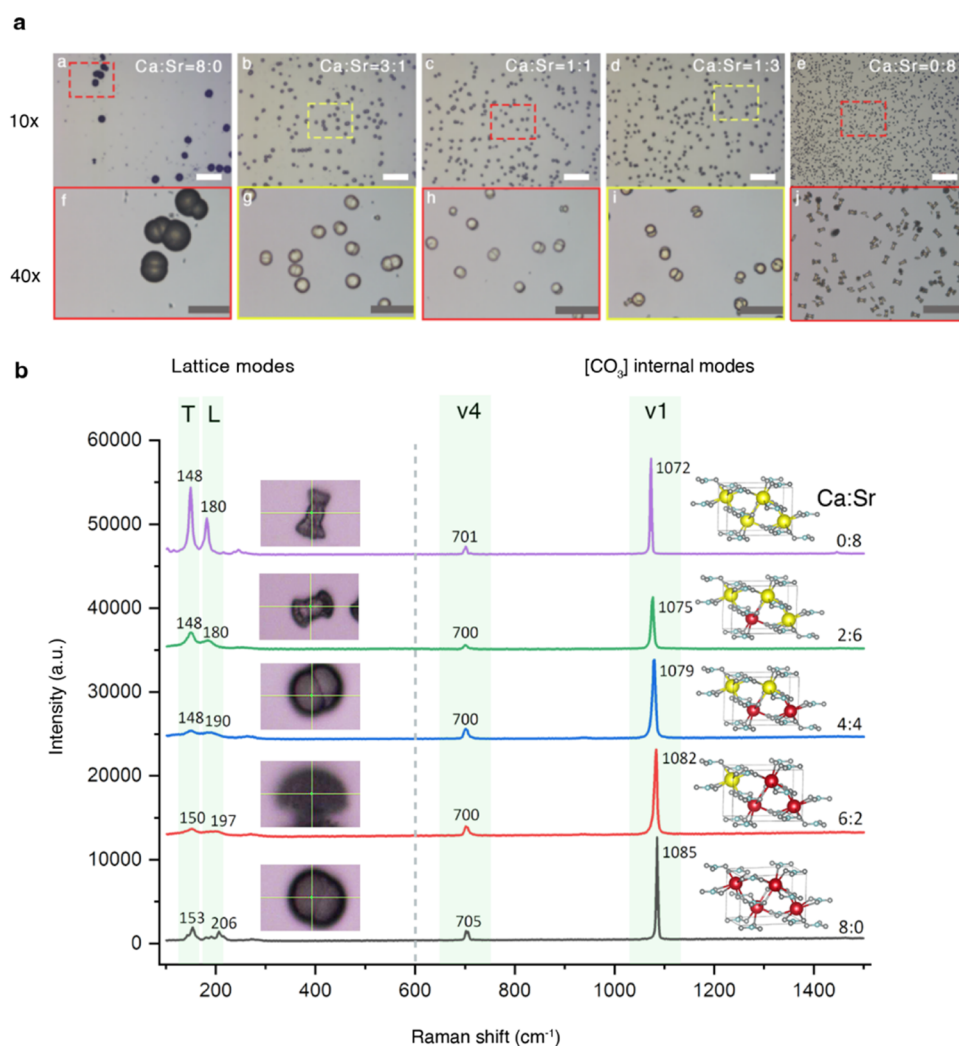
Figure 1. (a) Morphology and structure of crystals formed in the *in vitro* aragonite crystallization system with different Sr/Ca under an optical microscope. (b) Raman spectrum of the *in vitro* aragonite crystallization system; T, translation (lattice mode); L, libration (lattice mode); ν 4, in-plane bend (internal mode); ν 1, symmetric stretch (internal mode); scale bars: white, 100 μm; gray, 50 μm.

interference but ignored those associated with growth rates. To solve this problem, we propose a new experimental strategy in this research. The highlight of this method is semiquantitatively probing the growth rate of the nacreous layer by strontium (Sr) elements that belong to the same family as calcium. The crystal shape of both strontianite and aragonite is orthorhombic and belongs to the *Pmcn* space group.[20] The Raman result from our *in vitro* crystallization experiment showed that the strontium ions could replace a part of the calcium ions, forming isomorphic aragonite or intermediate crystals, such as $(Ca, Sr)[CO_3]$ or $(Sr, Ca)[CO_3]$. Many studies have also shown Sr deposits in the biominerals of various mollusks, including Mytilus, Giant Clam, snail, coral, and so on.[21-24] In 2009, Suzuki et al. detected the growth rate of nacre in *Pinctada fucata* by measuring the thickness between the surface of the nacreous layer and the strontium-labeled layer under a scanning electron microscope.[11] However, the sample size is limited when conducting these experiments, and the method is also not accurate enough. In addition, not all of the factors that play a pivotal role can cause a significant growth rate difference. Therefore, a qualitative description is insufficient to mitigate such effects and determine whether some elements affect the growth rate of the nacreous layer. In

response to these problems, we put forward the DCSr-NL method, a relative semiquantitative analysis for the growth rate of the shell nacre. Moreover, combined with the RNAi technology, researchers can quickly determine whether the matrix proteins or other genes have a regulatory effect on the growth rate of the shell nacre.

RESULTS

Isomorphism Induced by Strontium in Aragonite. As a member of the aragonite group, strontianite $Sr[CO_3]$ shares the same space groups and crystal systems as aragonite $Ca[CO_3]$.[25] To verify whether Sr can replace calcium particles in aragonite $Ca[CO_3]$ according to the presence or absence of isomorphism, the structure and morphology of crystals in the *in vitro* aragonite crystallization system with different ratios of Sr/Ca were detected with Raman spectra and observed under optical microscopes. With the increase in Sr^{2+} in the crystallization system, although the crystal size gradually became smaller, the crystal morphology formed in different experimental groups was uniform (Figure 1a), indicating that a single crystal could be formed at different concentrations of strontium calcium. Figure 2b shows that the peaks appeared at 1085, 705, 206, and 153 cm^{-1} are consistent with the standard
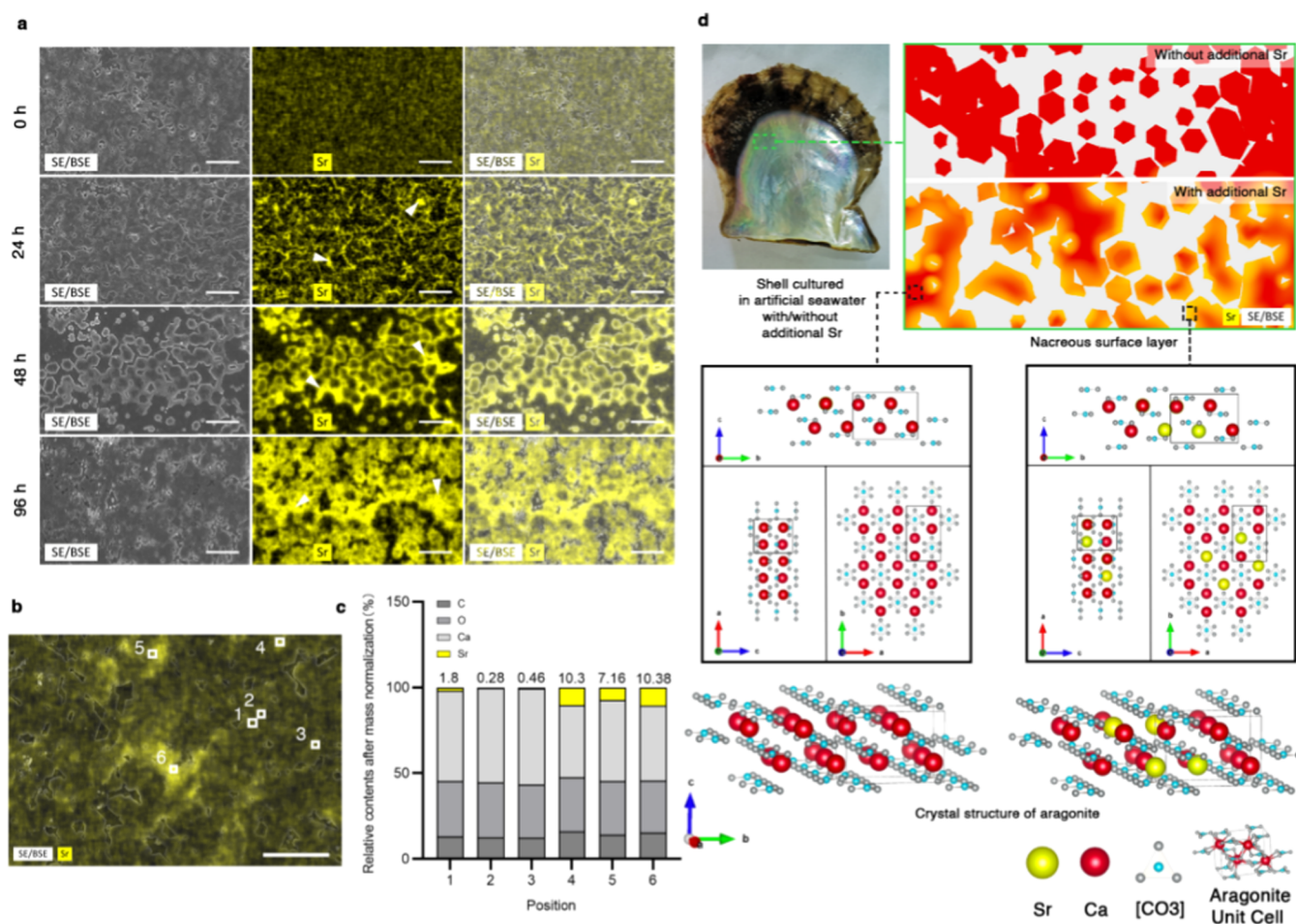
Figure 2. Labeling Sr on the nacre of pearl oyster. (a) Strontium distribution on the nacre surface at different time points. Line 1 is the nacreous surface morphology by SEM with BSE, line 2 shows the Sr distribution on the nacreous surface with SEM energy-dispersive X-ray spectroscopy (EDX), and line 3 is the merged graph of lines 1 and 2. The white arrowhead (bright yellow area) indicates the newly formed nacre labeled by Sr. (b) Strontium distribution on the nacreous surface after labeling for 24 h. White squares are the positions chosen to measure the relative contents of the four elements (C, O, Ca, and Sr). (c) Relative contents of C, O, Ca, and Sr from the six positions given in (b) after the mass normalization. The numbers on top of each column represent the relative percentages of the Sr element. (d) Schematic illustration for Sr labeling on the newly formed nacreous surface. Scale bar: 10 μm (a, b).

peaks of aragonite $Ca[CO_3]$ uploaded on the RRUFF database, whereas the peaks appeared at 1072, 701, 180, and 148 cm^{-1} are consistent with the standard peaks of strontianite $Sr[CO_3]$. With an increase in Sr^{2+} in the system, $\nu1$, $\nu4$, and the lattice vibration peaks of aragonite gradually shift from 1085, 705, 206, and 153 cm^{-1} to 1072, 701, 180, and 148 cm^{-1}, respectively, suggesting that the intermediate transition crystals, which are known to be isomorphic, including strontium-containing aragonite $(Ca, Sr)[CO_3]$ or calcium-containing strontianite $(Sr, Ca)[CO_3]$, may be formed (Figure 1b). These results provide the theoretical basis for our subsequent DCSr-NL method.

Marking the Nacreous Layer by the Strontium Element. To successfully label the newly formed shell nacre surface with the Sr element, we first cultured *P. fucata* in seawater with a specific Sr concentration. Then, we analyzed the distribution of Sr on the nacreous layer at different time points by backscattered electron imaging (BSE) and large-area energy-dispersive X-ray spectroscopy in SEM (SEM-EDX). The bright yellow part in the image represents the newly generated nacre after Sr marking (Figures 2a and S1). The results showed that, compared with 0 h, the bright yellow area

of the sample labeled for 6 h is a dot-like distribution, which turned into blocks at labeling times of 12 h and 24 h, and turned into flakes on the 2nd and 4th days. At the same time, according to the brightness of the color, we selected 4 and 6 points on the 6 and 24 h cultured samples, respectively (Figures S2a and 2b), and detected the relative contents of C, O, Ca, and Sr elements in these positions by energy-dispersive X-ray spectroscopy (EDX) in SEM. From the energy spectrum of different selected positions (Figures S2c and S3), we can intuitively see that C, O, Ca, and Sr have peaks with different signaling strengths at different positions. After a mass normalization analysis, we found that the Sr contents at positions 4, 5, and 6 in Figure 2b and positions 3 and 4 in Figure S2a are significantly higher than those in positions 1, 2, and 3 in Figure 2b and positions 1 and 2 in Figure S3, respectively (Figures 2c and S2b). Interestingly, the relative contents of calcium in each spectrum decreased, but the total amounts of Sr and Ca are relatively stable, suggesting that Sr can partially replace the deposition of Ca as the cultivation time increases. Figure 2d is a schematic diagram of the inner surface of the newly formed nacreous layer, which is marked with the strontium element. The red part is the unmarked area
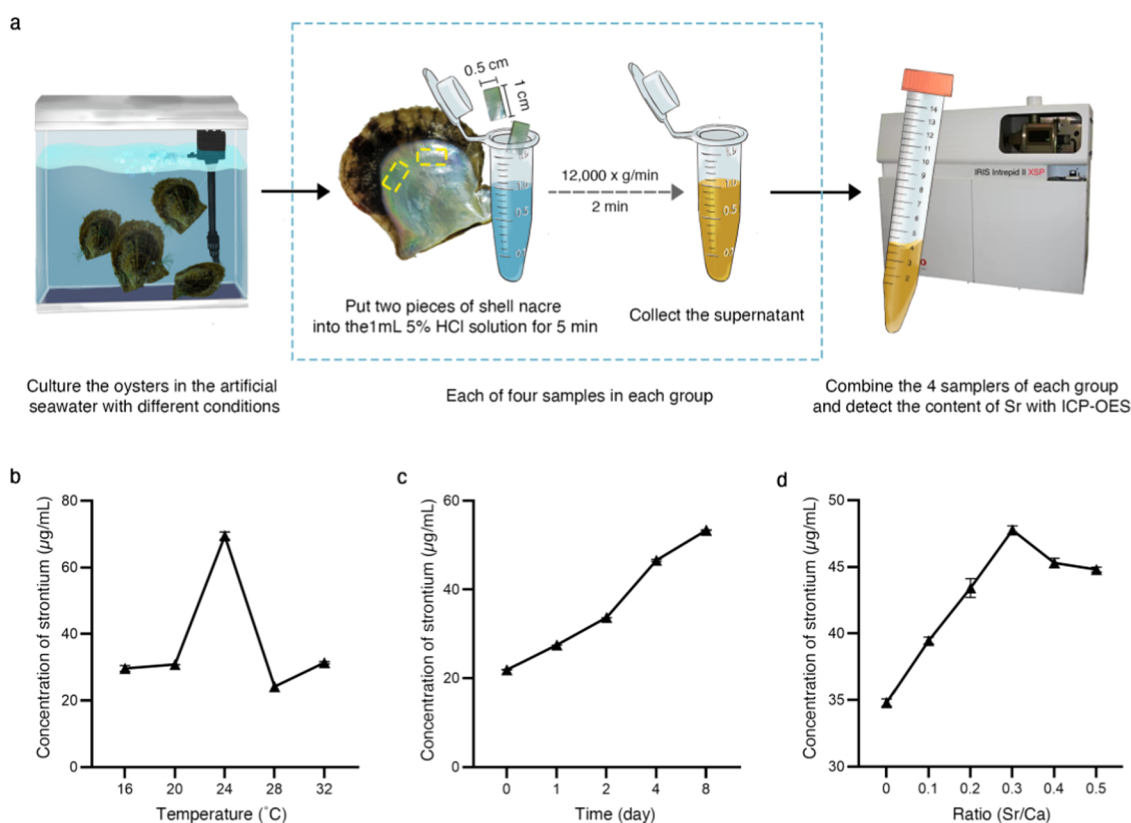
Figure 3. Workflow of optimal conditions for the DCSr-NL method. (a) Schematic of the DCSr-NL workflow for strontium content detection on the nacreous surface of the shell. (b) Sr concentrations of the newly formed nacre detected in seawater with different Sr/Ca ratios. (c) Sr concentrations of the newly formed nacre that was cultivated for different time periods. (d) Sr concentrations detected at different cultivation temperatures in the newly formed nacre. Each group of experiments used 4−5 oysters. Each value represents the mean ± standard deviation (SD) of triplicate measurements.

containing only Ca^{2+} in the aragonite lattice, and the orange part is the area where Sr^{2+} replaces a part of the Ca^{2+} in the lattice. Combined with Figure 2a, the Sr element is deposited on specific regions of the inner surface of the nacre and is not diffuse, suggesting that the deposition process of Sr is not haphazard but is biologically regulated. It also provides a theoretical foundation for estimating the growth rate of the nacre with DCSr-NL.

Detecting the Growth Rate of the Nacreous Layer under Different Conditions. The nacreous layer formation is a complex process affected by external factors, including temperature, pH, and salinity, and internal factors such as biomacromolecules.[26−29] Therefore, we explored the most suitable conditions for strontium labeling, such as the labeling time, the concentration of strontium in seawater, and the temperature, to ensure the accuracy of subsequent experiments. According to the flow chart of DCSr-NL (Figure 3a), we detected the concentrations of Sr under the different conditions mentioned above. The results showed that when the marking time is less than or equal to 4 days, the Sr/Ca is less than or equal to 0.3, and the concentration of Sr increases linearly. However, when the labeling time is greater than 4 days or Sr/Ca is greater than 0.3, the rate of increase in the Sr concentration slows down (Figure 3b,c). The detected concentration of strontium is the highest at 24 °C, where it is approximately 1.6−1.8 times that at other temperatures (Figure 3d). Thus, we conducted the subsequent experiment at 24 °C, with a Sr/Ca ratio of 0.3 and a cultivation cycle of about 4 days.

Exploring and Validating the Functions of Matrix Proteins Nacrein and Pif177. To test the efficacy of this method, we chose two well-studied matrix proteins (nacrein and Piff177) to conduct the subsequent experiments. Nacrein participates in nacre formation by saturating the partial Ca^{2+} and HCO_3^- due to its carbonic anhydrase domain that catalyzes HCO_3^- formation and its Gly-Xaa-Asn repeat domain that might combine with calcium ions.[30−32] Pif177 regulates nacre formation synergically by separating into pif80, which interacts with other matrix proteins, and pif97, which recruits pif80 after binding on chitin *via* its chitin-binding domain after translational modification.[11,33] The tissue distribution experiment results showed that the mRNA expression levels of nacrein and Pif177 are significantly high in the mantle tissue (Figures S4a,d). Interestingly, the mRNA expression level of Pif177 is extremely high in MC (Figure S4e), which was reported only in MP, ME, and the pearl sac, which might indicate as to why Pif177 exists in the pearl sac. Further detection across the tissue showed that nacrein has the highest expression level in MP (Figure S4b), which mutually corroborated with the known functions of nacrein and Pif177.

To verify the *in vivo* functions of the matrix proteins nacrein and Pif177, we injected a specific dsRNA (30 μg) to the adductor muscle of *P. fucata* to inhibit their expression levels, and observed the surface morphology and the growth rate of the shell nacre. The dsRNA (30 μg) of green fluorescent protein (GFP) was injected into the control group. Real-time PCR was performed to detect the mRNA expression levels of nacrein and Pif177 in MP. Compared with the control group,
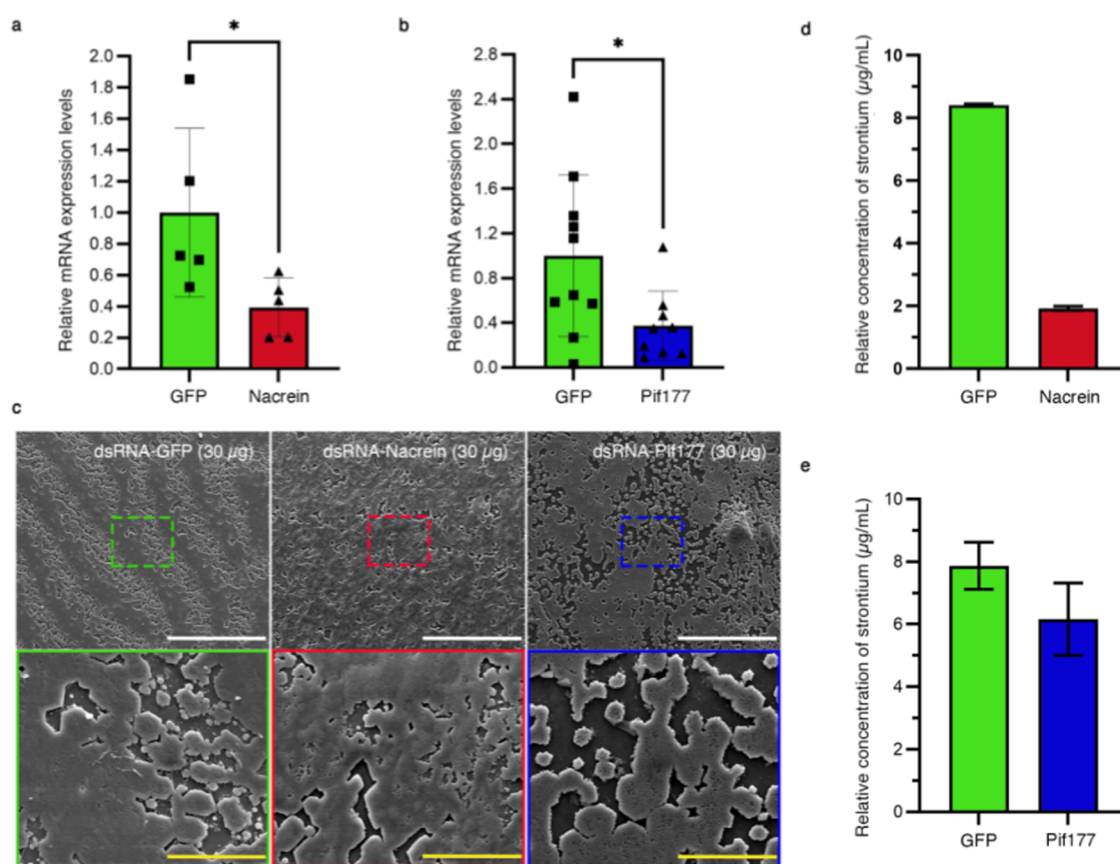
Figure 4. Study of the function of nacrein and Pif177 by combining RNAi with the DCSr-NL method. (a, b) Relative mRNA expression levels of nacrein and Pif177 in the MP at day 5 after dsRNA injection. The GFP group has a relative value of 1.0. Asterisk indicates a significant reduction (*$P < 0.05$, unpaired Student's t test) compared with dsRNA-GFP-injected oysters. (c) SEM images of the nacreous surface of the oysters injected with 30 μg of dsRNA-GFP, 30 μg of dsRNA-Nacrein, and 30 μg of dsRNA-Pif177, respectively. (d, e) Relative contents of Sr in the nacre of the oysters injected with 30 μg of dsRNA-GFP, 30 μg of dsRNA-Nacrein, and 30 μg of dsRNA-Pif177, respectively, were measured by DCSr-NL; five oysters ($n = 5$) were used in the dsRNA-Nacrein-injected group, and nine oysters ($n = 9$) were used in the dsRNA-Pif177-injected group; each value represents the mean ± SD of triplicate measurements. Scale bars: white, 10 μm; yellow, 50 μm.

the mRNA expression levels of nacrein and Pif177 were suppressed by approximately 40% (Figure 4a,b). The microstructure of nacre was observed by SEM. Although the inner surface morphology of the shell nacre injected with dsRNA-Nacrein was similar to that of the control group under a scanning electron microscope (Figure 4c), merely 1.92 μg mL^{-1} of deposition was detected compared with the control group, in which Sr accumulation was 8.4 μg mL^{-1} (Figure 4d), indicating that the suppression of the nacre growth rate by approximately 80% seems to yield no noticeable change in the surface structure. However, it was an entirely different case in the group injected with dsRNA-Pif177, in which the anomaly of the surface structure was significant (Figure 4c) despite the growth rate being suppressed by 20% (Figure 4e). This is consistent with reported studies. These results imply that our method can play a significant role in the quantitative assessment of the relative growth rate of the nacre.

Functions of MRPN, NU3, and NU9 during Nacre Formation as Revealed by DCSr-NL. To further verify the practicability of the DCSr-NL method, we studied the function of some new matrix proteins, MRPN, NU3, and NU9, which mainly exist in the nacre layers of *P. fucata*.[34] Their functions during mineralization are still unclear. The primers of NU3 and NU9 used to detect their tissue distributions were designed according to the full-length sequence obtained by RACE, and

those of MRPN were designed according to the partial sequence information (pfu_aug2.0_9281.1_06388) uploaded in *P. fucata* 2.0. The real-time PCR result showed that all of them were mainly expressed in the mantle tissue and were highly distributed in MP and MC (Figure S6), indicating that they might have a regulatory effect on the shell nacre formation.

To further explore their function during nacre formation *in vivo*, we knocked down their expression separately with an RNAi assay as in the case of nacrein and Pif177, and then detected the nacreous surface growth rate by the DCSr-NL method and observed the morphological changes under a scanning electron microscope. Compared with the control group injected with dsRNA-GFP, the mRNA expression levels of MRPN, NU3, and NU9 in each experimental group injected with 60 μg/200 μL of MRPN, NU3, and NU9 dsRNA significantly decreased in mantle tissues by 70, 60, and 40%, respectively (Figure 5a). Then, we detected the relative Sr content in the newly formed nacreous inner surface in each group by the semiquantitative DCSr-NL method. Compared with the control group, in which the Sr content is 8 μg/mL, the Sr contents in NU3, NU9, and MRPN dsRNA-injected groups decreased to 2, 4, and 3 μg/mL, respectively (Figure 5b). Therefore, inhibiting the relative expression levels of NU3, NU9, or MRPN would slow down the growth rate of the inner
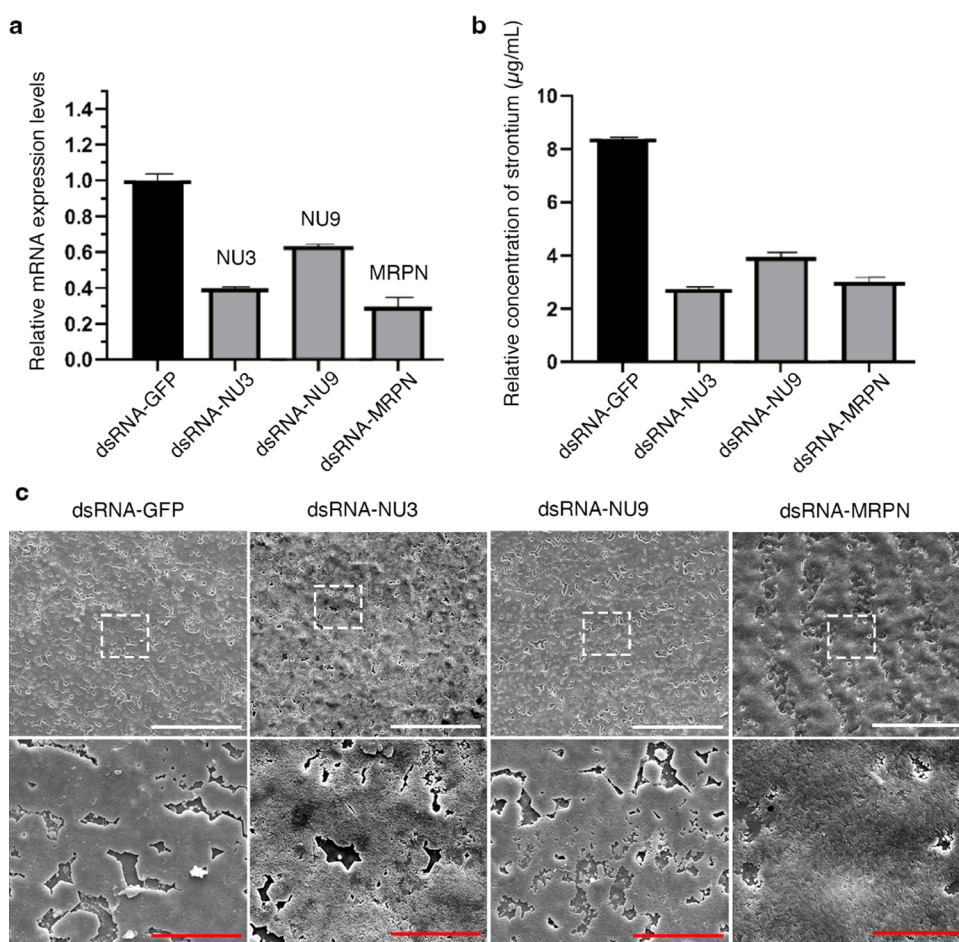
Figure 5. Study of the functions of NU3, NU9, and MRPN by combining RNAi with the DCSr-NL method. (a) Relative mRNA expression levels of NU3, NU9, and MRPN in the mantle tissue determined at day 5 after dsRNA-NU3, dsRNA-NU9, and dsRNA-MRPN injections. The dsRNA-GFP group has a relative value of 1.0. (b) Sr concentrations in the newly formed nacre detected by DCSr-NL from *P. fucata* injected with 60 μg of dsRNA-NU3, dsRNA-NU9, and dsRNA-MRPN, respectively. (c) Surface morphologies of nacre injected with 60 μg of dsRNA-GFP, dsRNA-NU3, dsRNA-NU9, and dsRNA-MRPN, respectively. Each group of experiments used 4−5 oysters, and each value represents the mean ± SD of triplicate measurements. Scale bar: white, 50 μm; red, 10 μm.

surface of the nacreous layer. However, no significant surface morphological change was observed in the dsRNA-NU9-injected group, and an illusion of enhanced growth was observed in the dsRNA-MRPN group. This suggests that the DCSr-NL method makes up for the shortcomings of the observation under a scanning electron microscope, which is inefficient at exploring the changes in the nacreous growth rate accurately, and provides new research ideas for studying the function of matrix proteins *in vivo*.

DISCUSSION

Both Strontium carbonate and aragonite belong to rhombohedral crystalline systems and are isomorphic. The results showed that strontium could deposit on the nacre surface during nacre formation by partially replacing the calcium on increasing the ratio of Sr/Ca in the seawater (Figures 2a and 3d). According to these properties, we established the DCSr-NL method (Figure S7d) to semiquantitatively measure the nacre growth rate by obtaining the strontium content deposited on the nacre surface with inductively coupled plasma optical emission spectroscopy (ICP-OES). The results from DCSr-NL showed that nacre formation was significantly inhibited when nacrein and Nu9 were knocked down, which showed no morphological changes under a scanning electron

microscope after injecting with dsRNA (Figures 4 and 5). Also, an illusion of enhanced growth was observed under a scanning electron microscope when injected with the dsRNA-MRPN (Figure 5). Thus, this method compensates for the shortcomings of the method proposed by Suzuki et al. (Figure S7a), which is only suitable for matrix proteins that cause significant morphological changes observable under a scanning electron microscope after injecting dsRNA.

Furthermore, to confirm whether increasing the strontium level in seawater affects the growth state of *P. fucata*, we measured the relative mRNA expression levels of the nacrein and Pif177 genes in mantle tissues by RT-qPCR. The results showed that no significant changes were detected at least up to 4 days after labeling (Figure 3c), indicating that a moderate increase in the Sr/Ca ratio of the seawater for a short period did not affect the growth state of the shells.

Based on the trend in the growth curve, the strontium content on the nacre surface was supposed to increase linearly with increasing culture time. However, the study of the optimal experimental conditions for strontium labeling showed that the strontium content at 8 days was less than twice as high as that at 4 days of labeling, indicating that aragonite deposition on the nacre surface has slowed. The nacre of shells comprises stacks of aragonite flakes that are about 500 nm thick, with a

framework of organic matter of about 30 nm thickness between each layer.[26] Therefore, it is also possible that the slower growth rate of the nacreous layer is due to the time required to form an organic framework after a certain extent of aragonite deposition.

The mantle tissue can be divided into the mantle edge, palial, and center according to the differentiation degree.[12] As the matrix proteins from ME are mainly involved in the prismatic layer formation, and those in the MP and/or MC are involved in nacre formations, MP and MC are not distinguishable when tissues are subjected to the detection of the relative mRNA expression levels. Although they both express matrix proteins primarily associated with nacre formation, there are significant differences in practice. Our results showed that the expression level of Pif177 is extremely high in MC (Figure S4e), which was reported only in MP, ME, and the pearl sac, indicating as to why Pif177 exists in the pearl sac.[36]

CONCLUSIONS

Due to the lack of suitable experimental techniques, the current functional investigations of matrix proteins rely primarily on *in vitro* functional experiments. In this study, a new method, DCSr-NL, is proposed, which can measure the growth rate of nacre. Combined with RNAi, it can be used to explore the effect of matrix proteins on the growth rate of nacre *in vivo*. Through this research approach, we explored the functions of the matrix proteins nacrein, Pif177, MRPN, NU3, and NU9. It was found that Pif177, MRPN, and NU3 all had regulatory effects on the morphology and growth rate of the nacreous layer, whereas nacrein and NU9 only regulated the growth rate of the nacreous layer and had no effect on the morphology. This shows that the DCSr-NL method considerably compensates for the shortcomings of using SEM to explore the growth rate of shells (Figure S7), which is of considerable significance for elucidating the roles of matrix proteins in the process of biomineralization.

MATERIALS AND METHODS

Specimen Preparation for Raman Spectroscopy. The total volume of the crystallization system is 20 μL, in which the final concentrations of $HCO_3-(NaHCO_3)$ and $Mg^{2+}(MgCl_2)$ ions were 16 and 50 mM, respectively. The total concentrations of $Ca^{2+}(CaCl_2)$ and Sr^{2+} ($SrCl_2$) were 8 mM. The ratios of Ca^{2+} and Sr^{2+} used in experiments were 1:0, 3:1, 1:1, 1:3, and 0:1. A 20 μL drop of the liquid was placed on the siliconized glass slide, put in a wet box, and reacted at room temperature for 48 h. The crystals were washed gently with Milli-Q water, dried in air, and analyzed by Raman spectroscopy and optical microscopy.

Animals and Culture Conditions. Adult pearl oysters, around 2-year-old, live, and healthy *P. fucata*, with a shell length of 5−6 cm and a wet weight of 30−40 g, were purchased from the Zhanjiang Pearl Farm (Guangdong, China) and cultured at 23−24 °C in a glass aquarium filled with 33‰ aerated artificial seawater (33 g PRO Reef Sea Salt in 1L water; http://www.qdseasalt.com/). The concentration of Ca^{2+} was about 440 mg/L. The oysters were fed with spirulina powder dissolved in seawater twice a week.

Strontium Distribution on the Surface of the Shell Nacre. After the shells were cleansed of adhering tissues, the nacreous layer specimens were collected from the junction between the nacreous and prismatic layers (Figure 3a) and

dried naturally. Then, the dried specimens were fixed on the SEM sample stage with a conductive carbon tape and coated with palladium in the sputter coater instrument according to the manufacturer's instructions (HITACHI E-1010 ion sputtur, coating parameters used: vacuum 10 Pa high sputtering voltage, current 16 mA, coating time 60 s). Finally, the Sr distribution on the surface of specimens was detected by combining BSE with SEM-EDX under a field-emission scanning electron microscope (HITACHI SU8220, 10 kV, 2500×).

Relative Contents of Different Elements on the Same Position. The relative contents of C, O, Ca, and Sr were measured and analyzed by energy-dispersive X-ray spectroscopy (SEM-EDX).

Content of Strontium in the Shell. We washed the shell as clean as possible with water after removing adhering tissues. Next, the prismatic layer, which is the outer layer of the shell, was ground. Then, two tablets of 0.5 cm × 1 cm were taken from each shell at the border between the nacreous and prismatic layers on the inner surface of the shell. Next, 1 mL of 5% hydrochloric acid was added to every two pieces of 1 cm × 0.5 cm nacre tablets and reacted for 5 min. Then, the residue was discarded after centrifuging at 12,000g min^{-1} for 2 min. Finally, supernatants from the same group were combined, and the growth rate of shell nacre was quantified by detecting the Sr concentration in the solution by ICP-OES (plasma emission spectrometer).

Time-Gradient Experiment. To prepare the artificial seawater with a suitable Sr/Ca ratio of 0.3, we dissolved 1.76 g of $SrCl_2·6H_2O$ in 5 L of artificial seawater. The oxygen pump was opened, and the artificial seawater was maintained under constant aeration at 24 °C for 24 h. The oysters were then left in the aquarium and fed with small amounts of spirulina powder dissolved in seawater. Five oysters were taken as specimens each time at 0, 6, 12, 24 h, 1, 2, 4, and 8 days.

Note: Precipitation was observed when the mole ratio of Sr and Ca was greater than or equal to 0.6 at RT.

Concentration-Gradient Assay of Sr Labeling. We dissolved 0, 0.293, 0.5866, 0.88, 1.174, and 1.466 g L^{-1} $SrCl_2·6H_2O$ in 5 L of artificial seawater in 7 L fish aquariums to obtain the special artificial seawater with the mole ratios between Sr and Ca of 0, 0.1, 0.2, 0.3, 0.4, and 0.5, respectively. The oxygen pump was opened, and the special artificial seawater was maintained under constant aeration at 24 °C for 24 h. Five healthy oysters were placed in each aquarium and fed with small amounts of spirulina powder dissolved in seawater. The Sr contents of specimens were measured by the abovementioned method on day 4.

Temperature-Gradient Assay of Sr Labeling. We prepared 30 L of special artificial seawater, in which the mole ratio of Sr and Ca was 0.3, and aliquoted it into six 7 L fish aquariums. The oxygen pump was opened, and the seawater was maintained under constant aeration at 24 °C for 24 h. Then, the temperature of aquariums was reset to 16, 20, 24, 28, and 32 °C, respectively. Five healthy oysters were placed in each aquarium when the temperature was stable. The oysters were fed with small amounts of spirulina powder dissolved in seawater. The Sr contents of specimens were measured by the abovementioned method on day 4.

RNA Extraction from *P. fucata*. Total RNA was extracted from the tissue using the standard protocol for TRIzol reagent (Invitrogen, Code No: 15596018) for general cloning of genes. The RNA concentration was measured with a NanoDrop2000

at 260 nm (Life Technologies, Thermo). The quality and quantity of RNA were determined by measuring the OD260/280, OD260/230, and OD260 with a NanoDrop Lite spectrophotometer (Thermo Scientific).

Acquisition and Analysis of Full-length cDNA Sequences of NU3 and NU9. The partially known sequences of NU3 (pfu_aug1.0_2111.1_22872) and NU9 (pfu_aug1.0_4561.1_44973) are from the database *P. fucata* ver. 1.0 + 1.1 (https://marinegenomics.oist.jp/pearl/viewer/info?project_id=20). The full-length cDNA sequences of NU3 and NU9 were obtained by the SMARTerTM RACE cDNA Amplification Kit (Code No. 634858/59, Clontech). The primers NU3-GSP1 and NU9-GSP1 were used for 5′RACE and NU3-GSP2 and NU9-GSP2 were applied to 3′RACE, respectively. The NU3 and NU9 gene sequences were submitted to the ORF finder website (https://www.ncbi.nlm.nih.gov/orffinder/) to obtain the opening reading frame sequence, and the signal peptide was analyzed by SignalP-5.0 Server (http://www.cbs.dtu.dk/services/SignalP/). The putative protein sequence was predicted online with the ExPASy Translate tool (https://web.expasy.org/translate/)

NU3-GSP1 CATTGGCCATATGCCTCTCTGTCC
NU3-GSP2 CTTCAGAGAAGAGCCAATGAAGGCTC
NU9-GSP1 AGGTCAACTTCTGCTTGTTCGCGC
NU9-GSP2 AGGGTTCAAGTTCGACTTGGAGCC
UPM-short: CTAATACGACTCACTATAGGGC
UPM-long: CTAATACGACTCACTATAGGGCAAG-CAGTGGTATCAACGCAGAGT

Tissue Distributions Detected by Real-Time PCR. The primers utilized to detect nacrein, Pif177, and MRPN were prepared based on the nucleotide sequences from Genbank (Genbank ID: D83523 and AB236929), whereas primers for NU3 and NU9 were based on the full-length sequence mentioned above. GAPDH is treated as a reference gene of qPCR. The primers are shown below:

Nacrein-RT-F: CACACCTATGGAGGCTCATTTGG;
Nacrein-RT-R: AGCCGTCATCTCCGACCTCAAG;
Pif177-RT-F: CGAGATAGAGAGCATAGCATATG;
Pif177-RT-R: ACTTTGGGCTTCTTAGCTTTG;
NU3-RT-F: GGAAGCAGTAGGACCTGCAATCG
NU3-RT-R: GCCTTCATTGGCTCTTCTCTGAAG
NU9-RT-F: CGTGCGTCTATCTTGAGGAATGC
NU9-RT-R: CTGCTGGTCTAGTCTCTGGAGAAG
MRPN-RT-F GGGACCTATGGGCATAATGAG
MRPN-RT-R ATGTCGAACCCACCGATCATACC
GAPDH-RT-F: TTTTGGCATTGAGGAAGGTTTG
GAPDH-RT-R: CAGTGGAGGATGGTATGATGTTAG.

The foot, gonad, gill, viscus, adductor muscle, mantle, mantle pallial, mantle edge, and mantle center were collected from three to five oysters as specimens, and the total RNA was extracted by the abovementioned method. First, 1 μg of reverse-transcribed total RNA with RT Master Mix (Takara; Code NO: RR036A) was taken. Then, the 10-fold diluted transcription product was used as the template for the following real-time PCR with Premix Ex Taq (Takara; Tli RNaseH Plus; Code NO: RR420A). Finally, the real-time PCR for nacrein, Pif177, NU3, NU9, and MRPN detection was performed according to the manufacturer's instructions in a LightCycler 480 system, in which GAPDH was chosen as the reference gene.

We used three technical replicates per sample to limit the impact of measurement errors. All PCR products were subcloned and verified by sequencing. Cycle threshold (Ct)

values were calculated in each reaction and normalized to the internal control (GAPDH). The relative mRNA expression level of the gene of interest was calculated using the comparative Ct method. The graphing software used is GraphPad Prism 9.

RNAi Experiment. The *in vivo* RNAi assay was conducted as described by Suzuki et al.,[11] with some modifications.

Double-Strand RNA (dsRNA) Designation. We referred to the manufacturer's instruction in the Large Scale RNA Production Systems−T7 (Promega, Code NO: P1300) kit to design double-stranded RNAs (dsRNAs). DsGFP, as a negative control, was designed by referring to Vector pEGF-N1 (NEB). The sequences are as shown below:

RNAi-Nacrein-F: GCGTAATACGACTCACTATAGGGA-GAATGCAGAAATTGATTCTAGCTG;
RNAi-Nacrein-R: GCGTAATACGACTCACTATAGGGA-GAATCCTCTGTCTCCTCAACGTC;
RNAi-Pif177-F: GCGTAATACGACTCACTATAGGGA-GAAAGGGTCATGCAAGTTCCATCT;
RNAi-Pif177-R: GCGTAATACGACTCACTATAGGGA-GATGCATAGATAATCAGGGATTTC;
RNAi-NU9-F: GCGTAATACGACTCACTATAGGGA-GAGCAGTAGGACCTGCAATCGAC;
RNAi-NU9-R: GCGTAATACGACTCACTATAGGGA-GAAACTGGTAGGTTGCAGTGTAATTC
RNAi-NU3-F: GCGTAATACGACTCACTATAGGGA-GAGCAGTAGGACCTGCAATCGAC;
RNAi-NU3-R: GCGTAATACGACTCACTATAGGGA-GACGATGACGCCACTCAGATCAG;
RNAi-MRPN-F: GCGTAATACGACTCACTATAGGGA-GAGCGAAGGATACTGTGTTTGTTCG;
RNAi-MRPN-R: GCGTAATACGACTCACTATAGGGA-GACCATGTGTCCTCCTAACTATCATG;
RNAi-GFP-F: GGATCCTAATACGACTCACTATAG-GATGGTGAGCAAGGGCGA;
RNAi-GFP-R: GGATCCTAATACGACTCACTATAG-GACTTGTACAGCTCGTCCATG.

Double-Stranded RNA Synthesis. A standard 50 μL PCR reaction was performed with Super-Fidelity DNA Polymerase (Vazyme, Code No: P501), using the primers mentioned above, which were designed to amplify the cDNA fragments of nacrein, Pif177, NU3, NU9, and MRPN and GFP with an additional T7 promoter sequence at both 3′ and 5′ ends. The templates for each standard PCR reaction, except the amplification of GFP-cDNA, were generated from the total RNA of the mantle pallial. The cDNA fragment of GFP was amplified from Vector pEGF-N1(NEB). Finally, dsRNAs of each of the genes were obtained with the Large Scale RNA Production Systems-T7 kit (Promega, Code No: P1300) by transcribing the amplified cDNA that was extracted by the DNA Gel Extraction Kit (Vazyme, Code No: DC301). The concentration of RNA duplex was measured using ultraviolet (UV) absorbance at 260 nm after resuspending in an appropriate amount of RNase-free distilled water and then diluted into 30 μg per 200 μL at 4 °C.

Double-Stranded RNA Injection. Animals were handled and experiments were conducted according to the national regulations after approval by the local experiments ethical committee.

Regardless of the amount of dsRNA applied, the volume of injection was 200 μL throughout this study. The pearl oyster used for this experiment had a 5−6 cm shell length and was anesthetized in the commercial artificial seawater with 2‰ 1,4-

diphenoxybenzene (Aladdin, Code No: P135297) before injection. Samples were injected by inserting a sterilized needle (1 mL) into the adductor muscle. Then, they were reared in the artificial seawater with a Sr/Ca ratio of 0.3 for 5 days, after placing treated shells into the commercial artificial seawater for 24 h. The temperature was maintained around 23−24 °C.

DsRNA Efficiency Detection. The RNAi efficiency was detected by RT-PCR after extracting the total RNA from the mantle tissue. Then, the growth rate and morphological changes of the inner surface of the nacreous layer were detected by the DCSr-NL method and SEM, respectively.

■ ASSOCIATED CONTENT

ⓢ Supporting Information

The Supporting Information is available free of charge at https://pubs.acs.org/doi/10.1021/acsomega.2c02230.

Sr distribution of the nacreous inner surface after 6 and 24 h of cultivation in the artificial seawater (Sr/Ca = 0.3); element content on the nacreous inner surface; energy spectrum of six positions displayed in Figure 2b; relative mRNA expressions of nacrein and Pif177; full-length sequences of NU3 and NU9; tissue distributions of NU3, NU9, and MRPN; schematic comparison of the DCSr-NL method with Suzuki's method (PDF)

■ AUTHOR INFORMATION

Corresponding Author

Rongqing Zhang − *Ministry of Education Key Laboratory of Protein Sciences, School of Life Sciences, Tsinghua University, Beijing 100084, P. R. China;* Present Address: Department of Biotechnology and Biomedicine, Yangtze Delta Region Institute of Tsinghua University, Jiaxing, Zhejiang 314006, China; ⓞ orcid.org/0000-0001-9292-446X; Email: rqzhang@tsinghua.edu.cn

Authors

Li Yi − *Ministry of Education Key Laboratory of Protein Sciences, School of Life Sciences, Tsinghua University, Beijing 100084, P. R. China;* Present Address: Department of Biotechnology and Biomedicine, Yangtze Delta Region Institute of Tsinghua University, Jiaxing, Zhejiang 314006, China; ⓞ orcid.org/0000-0001-9131-4600

Bing Zou − *Ministry of Education Key Laboratory of Protein Sciences, School of Life Sciences, Tsinghua University, Beijing 100084, P. R. China;* Present Address: Department of Biotechnology and Biomedicine, Yangtze Delta Region Institute of Tsinghua University, Jiaxing, Zhejiang 314006, China

Liping Xie − *Ministry of Education Key Laboratory of Protein Sciences, School of Life Sciences, Tsinghua University, Beijing 100084, P. R. China*

Complete contact information is available at:
https://pubs.acs.org/10.1021/acsomega.2c02230

Author Contributions

L.Y. and B.Z. conceptualized the project. L.Y. and B.Z. designed, managed, and performed experiments. L.Y. performed data analysis and contributed to the figures. B. Z. acquired optical microscopy and SEM images. L.Y. and B.Z. contributed equally to this work. R.Z. and L.X. acquired funding and provided direction throughout the project. L.Y. and B.Z. wrote the manuscript. L.X. and R.Z. revised the manuscript.

Notes

The authors declare no competing financial interest.

■ REFERENCES

(1) Jackson, A. P.; Vincent, J. F. V.; Turner, R. M. The Mechanical Design of Nacre. *Proc. R. Soc. London, Ser. B* **1988**, *234*, 415−440.

(2) Belcher, A. M.; Wu, X. H.; Christensen, R. J.; Hansma, P. K.; Stucky, G. D.; Morse, D. E. Control of crystal phase switching and orientation by soluble mollusc-shell proteins. *Nature* **1996**, *381*, 56−58.

(3) Gao, H. L.; Chen, S. M.; Mao, L. B.; Song, Z. Q.; Yao, H. B.; Colfen, H.; Luo, X. S.; Zhang, F.; Pan, Z.; Meng, Y. F.; et al. Mass production of bulk artificial nacre with excellent mechanical properties. *Nat Commun.* **2017**, *8*, No. 287.

(4) Mao, L. B.; Gao, H. L.; Yao, H. B.; Liu, L.; Colfen, H.; Liu, G.; Chen, S. M.; Li, S. K.; Yan, Y. X.; Liu, Y. Y.; Yu, S. H. Synthetic nacre by predesigned matrix-directed mineralization. *Science* **2016**, *354*, 107−110.

(5) Mayer, G. Rigid biological systems as models for synthetic composites. *Science* **2005**, *310*, 1144−1147.

(6) Meyers, M. A.; Lin, A. Y. M.; Chen, P. Y.; Muyco, J. Mechanical strength of abalone nacre: Role of the soft organic layer. *J. Mech. Behav. Biomed. Mater.* **2008**, *1*, 76−85.

(7) Meyers, M. A.; McKittrick, J.; Chen, P. Y. Structural Biological Materials: Critical Mechanics-Materials Connections. *Science* **2013**, *339*, 773−779.

(8) Farre, B.; Dauphin, Y. Lipids from the nacreous and prismatic layers of two Pteriomorpha Mollusc shells. *Comp. Biochem. Physiol., Part B: Biochem. Mol. Biol.* **2009**, *152*, 103−109.

(9) Xiang, L.; Su, J. T.; Zheng, G. L.; Liang, J.; Zhang, G. Y.; Wang, H. Z.; Xie, L. P.; Zhang, R. Q. Patterns of Expression in the Matrix Proteins Responsible for Nucleation and Growth of Aragonite Crystals in Flat Pearls of *Pinctada fucata*. *PLoS One* **2013**, *8*, No. e66564.

(10) Marin, F.; Luquet, G.; Marie, B.; Medakovic, D. Molluscan Shell Proteins: Primary Structure, Origin, and Evolution. In *Current Topics in Developmental Biology*; Elsevier, 2007; Vol. *80*, pp 209−276.

(11) Suzuki, M.; Saruwatari, K.; Kogure, T.; Yamamoto, Y.; Nishimura, T.; Kato, T.; Nagasawa, H. An Acidic Matrix Protein, Pif, Is a Key Macromolecule for Nacre Formation. *Science* **2009**, *325*, 1388−1390.

(12) Fougerouse, A.; Rousseau, M.; Lucas, J. S. Soft Tissue Anatomy, Shell Structure and Biomineralization. In *The Pearl Oyster*; Elsevier, 2008; pp 77−102.

(13) Takeuchi, T.; Endo, K. Biphasic and dually coordinated expression of the genes encoding major shell matrix proteins in the pearl oyster *Pinctada fucata*. *Mar. Biotechnol.* **2006**, *8*, 52−61.

(14) Falini, G.; Albeck, S.; Weiner, S.; Addadi, L. Control of aragonite or calcite polymorphism by mollusk shell macromolecules. *Science* **1996**, *271*, 67−69.

(15) Sugawara, A.; Kato, T. Aragonite $CaCO_3$ thin-film formation by cooperation of Mg^{2+} and organic polymer matrices. *Chem. Commun.* **2000**, 487−488.

(16) Addadi, L.; Weiner, S. Biomineralization - A pavement of pearl. *Nature* **1997**, *389*, 912−913.

(17) Sugawara, A.; Oichi, A.; Suzuki, H.; Shigesato, Y.; Kogure, T.; Kato, T. Assembled structures of nanocrystals in polymer/calcium carbonate thin-film composites formed by the cooperation of chitosan and poly(aspartate). *J. Polym. Sci., Part A: Polym. Chem.* **2006**, *44*, 5153−5160.

(18) Yan, Y.; Yang, D.; Yang, X.; Liu, C.; Xie, J.; Zheng, G. L.; Xie, L. P.; Zhang, R. Q. A Novel Matrix Protein, PfY2, Functions as a Crucial Macromolecule during Shell Formation. *Sci. Rep.* **2017**, *7*, No. 6021.

(19) Chen, Y.; Gao, J.; Xie, J.; Liang, J.; Zheng, G. L.; Xie, L. P.; Zhang, R. Q. Transcriptional regulation of the matrix protein Shematrin-2 during shell formation in pearl oyster. *J. Biol. Chem.* **2018**, *293*, 17803−17816.

(20) De Villiers, J. P. R. Crystal Structures of Aragonite, Strontianite, and Witherite. *Am. Mineral.* **1971**, *56*, 758−767.

(21) Dodd, J. R. Environmental Control of Strontium and Magnesium in Mytilus. *Geochim. Cosmochim. Acta* **1965**, *29*, 385−398.

(22) Bonham, K. Growth Rate of Giant Clam *Tridacna gigas* at Bikini Atoll as Revealed by Radioautography. *Science* **1965**, *149*, 300−302.

(23) Rosenthal, G. M.; Nelson, D. J.; Gardiner, D. A. Deposition of Strontium and Calcium in Snail Shell. *Nature* **1965**, *207*, 51−54.

(24) Greegor, R. B.; Pingitore, N. E.; Lytle, F. W. Strontianite in coral skeletal aragonite. *Science* **1997**, *275*, 1452−1454.

(25) Klein, C.; Hurlbut, C. S. *Manual of Mineralogy*, 21st ed.; Academic Press: Wiley, 1993; p 681.

(26) Addadi, L.; Joester, D.; Nudelman, F.; Weiner, S. Mollusk shell formation: A source of new concepts for understanding biomineralization processes. *Chem. - Eur. J.* **2006**, *12*, 980−987.

(27) Latchere, O.; Mehn, V.; Gaertner-Mazouni, N.; Le Moullac, G.; Fievet, J.; Belliard, C.; Cabral, P.; Saulnier, D. Influence of water temperature and food on the last stages of cultured pearl mineralization from the black-lip pearl oyster Pinctada margaritifera. *PLoS One* **2018**, *13*, No. e0193863.

(28) Grenier, C.; Román, R.; Duarte, C.; Navarr, J. M.; Rodriguez-Navarro, A. B.; Ramajo, L. The combined effects of salinity and pH on shell biomineralization of the edible mussel Mytilus chilensis. *Environ. Pollut.* **2020**, *263*, No. 114555.

(29) Mann, S. Molecular Recognition in Biomineralization. *Nature* **1988**, *332*, 119−124.

(30) Miyamoto, H.; Miyashita, T.; Okushima, M.; Nakano, S.; Morita, T.; Matsushiro, A. A carbonic anhydrase from the nacreous layer in oyster pearls. *Proc. Natl. Acad. Sci. U.S.A.* **1996**, *93*, 9657−9660.

(31) Suzuki, M.; Nagasawa, H. Mollusk shell structures and their formation mechanism. *Can. J. Zool.* **2013**, *91*, 349−366.

(32) Yang, D.; Yan, Y.; Yang, X.; Liu, J.; Zheng, G. L.; Xie, L. P.; Zhang, R. Q. A basic protein, N25, from a mollusk modifies calcium carbonate morphology and shell biomineralization. *J. Biol. Chem.* **2019**, *294*, 8371−8383.

(33) Bahn, S. Y.; Jo, B. H.; Hwang, B. H.; Choi, Y. S.; Cha, H. J. Role of Pif97 in Nacre Biomineralization: In Vitro Characterization of Recombinant Pif97 as a Framework Protein for the Association of Organic-Inorganic Layers in Nacre. *Cryst. Growth Des.* **2015**, *15*, 3666−3673.

(34) Liu, C.; Li, S. G.; Kong, J. J.; Liu, Y. J.; Wang, T. P.; Xie, L. P.; Zhang, R. Q. In-depth proteomic analysis of shell matrix proteins of *Pinctada fucata. Sci. Rep.* **2015**, *5*, No. 17269.